Analysis of beam slowing-down process in large helical device based on Fokker Planck operator including beam beam Coulomb collision effect

Analysis of beam slowing-down process in LHD based on Fokker-Planck operator including beam-beam Coulomb collision effect

H Nuga[1], R Seki[1,2], S. Kamio[1], K. Ogawa[1,2], M. Isobe[1,2], M. Osakabe[1,2], M. Yokoyama[1,2], and LHD Experiment Group[1]

[1] National Institute for Fusion Sciences, National Institutes of Natural Sciences, Toki, Japan

[2]SOKENDAI (The Graduate University for Advanced Studies), Toki, Japan

E-mail: nuga.hideo@nifs.ac.jp

April 2018

Abstract. The contribution of the beam-beam (b-b) Coulomb collision effect to the fast ion slowing down process is investigated. The effect is evaluated experimentally in the Large Helical Device (LHD) from the response of the neutron emission rate to the direction of the tangential hydrogen beam, which is used with the tangential deuterium beam. In addition, to analyze the experimental results, a Fokker-Planck code is improved. It is observed that the decay time of the neutron emission rate after the deuterium beam is turned off depends on the direction of the hydrogen beam. This trend can be explained by the b-b Coulomb collision effect. The hydrogen beam, which has the same direction of the deuterium beam, deforms the fast deuteron velocity distribution due to the b-b Coulomb collision. As a result, the neutron decay time becomes longer than that with the opposite direction hydrogen beam. Our Fokker-Planck simulation shows that the b-b Coulomb collision effect contributes to the decay time of the neutron emission rate. This simulation result is qualitatively similar to the experimental result. For the quantitative analysis, consideration of the fast ion spatial transport, which is neglected in the present simulation, is required.

Keywords: Fokker-Planck, beam-beam Coulomb collision, neutron emission rate
Submitted to: *Nucl. Fusion*

1. Introduction

Achieving high confinement of the energetic particle (EP) confinement is one of the most important issues for fusion devices. Although the self-sustained plasma by fusion-born alpha particles is necessary to realize fusion reactors, the confinement performance of EPs is often degraded by several phenomena, such as neo-classical transport and instabilities driven by EP itself. Therefore, the confinement property of EPs with EP driven instabilities have been investigated in several experiments and simulations[1, 2, 3, 4, 5]. It is known that classical models, which assume no wave-induced EP transport, can not describe EP confinement accurately if the EP population is large enough to drive toroidal Alfvén eigen modes. Since the instabilities depend on the velocity and spatial space distribution of EPs, the estimation of the distribution is important for the EP transport analysis.

In fusion plasmas, there are several EP sources, such as fusion reaction, neutral beam injection (NBI), and radio frequency (RF) waves. EPs generated by different mechanisms may interact with each other due to the beam-beam (b-b) Coulomb collision, which is the Coulomb collision interaction between non-thermal particles, if their relative velocity is sufficiently small. Here, the term "b-b Coulomb collision" indicates not only the Coulomb collision between beam particles but also the collision between non-thermal particles. For example, we consider ITER and DEMO. The velocity of a 3.5 MeV alpha particle, which is generated by deuteron-deuteron (D-D) fusion reaction, is similar to that of a 1 MeV deuterium beam particle though its kinetic energy is three times greater than that of the beam particle.

Figure 1 is a simple example of the velocity distribution of deuteron and α particle in a steady state ITER-like plasma including and excluding the b-b Coulomb collision effect calculated by TASK/FP[6, 7]. Deuteron has a 1 MeV tangential NBI source and alpha particle has a 3.5 MeV isotropic particle source assuming deuteron-triton (D-T) fusion reaction. It is assumed that the bulk temperature and density, NBI absorption power, and fast α particle deposition power is constant and uniform in this calculation. To emphasize the b-b Coulomb collision effect, low collisionality plasma is chosen (electron bulk density $n_e = 2 \times 10^{19}$ m^{-3} and bulk temperature $T_e = 10$ keV). When the b-b Coulomb collision effect is neglected, the velocity distribution of α particle becomes an isotropic distribution (fig. 1-(d)) because the fast α particle source is assumed to be an isotropic. On the other hand, in the case including the b-b Coulomb collision effect, the velocity distribution of alpha particles (fig 1-(b)) is distorted into an anisotropic distribution since only alpha particles whose pitch angles are similar to that of deuterium beam are affected by the b-b Coulomb collision. Therefore, EP velocity distribution should be estimated including the b-b Coulomb collision effect because the distorted velocity distribution of alpha particles could result in a positive gradient in the velocity space (see $P_{para} \sim 5$, $P_{perp} \sim 0$ in fig. 1-(c)), which may excite instabilities driven by EPs.

The behavior of NB fast ions in the Large Helical Device (LHD) has been often

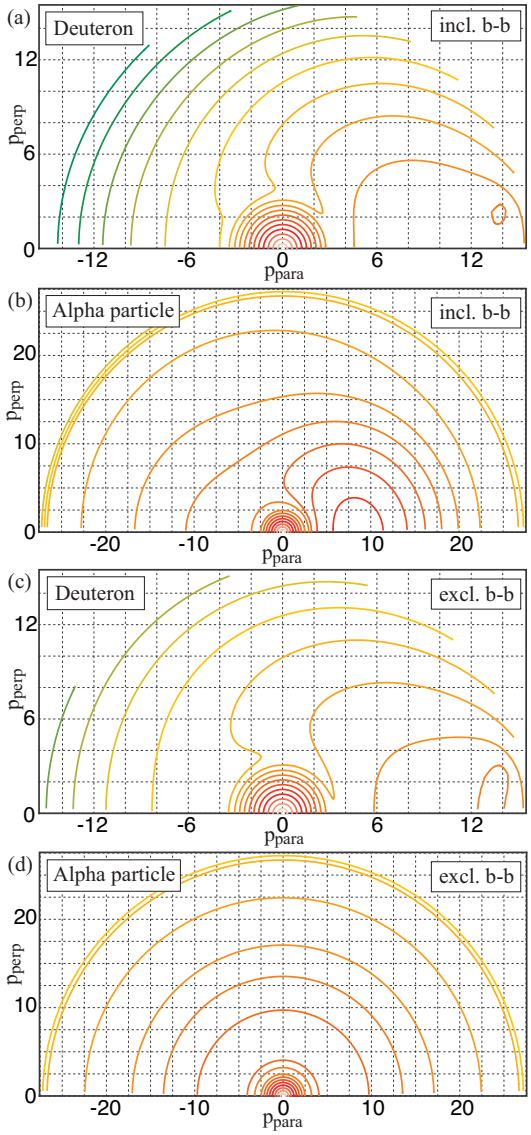

Figure 1. Conceptional image of the b-b Coulomb collision between deuteron NBI and fusion born alpha particle. Figures (a) and (b) show the momentum distribution function of deuteron with tangential NBI and alpha particles with isotropic EP source including the b-b Coulomb collision effect and figures (c) and (d) show those excluding the b-b Coulomb collision effect. Horizontal and vertical axes denote the momentum parallel and perpendicular to the magnetic field. The value of the momentum is normalized to the thermal momentum $p_i^{\rm th} = \sqrt{m_i T_i}$. Here, the subscript i indicates particle species.

analyzed by using five-dimensional drift kinetic Monte Carlo code GNET[8, 9, 10, 11]. Although the GNET code can analyze the behavior of fast ions accurately including the b-b Coulomb collision and the finite orbit width effect, however, GNET code consumes significant computational resources and calculation time. In the view of the experimental analysis, the rapid but sufficiently accurate code which calculates the evolution of the fast ion velocity distribution is required. Fokker-Planck (F-P) codes usually satisfy this requirement. Although F-P codes have difficulty including the finite orbit width effect unlike Monte Carlo codes, F-P codes require less computational resources and thus F-P codes are suitable for the analysis of a substantial amount of experiment data. For this reason, several F-P codes have been developed to simulate the behavior of fast ions[12, 13, 14, 15, 16, 17]. In the present research, to investigate the fast ion behavior, we have extended the three-dimensional (2D in momentum space and 1D in radial direction) F-P simulation code TASK/FP, which is a F-P component of the integrated code TASK[18] and TASK3D-a[19]. Although TASK/FP has been developed originally as a full velocity distribution (full-f) prediction code, in this extension, TASK/FP is modified to analyze experimental data as below. It is assumed that the ion velocity distribution f is divided into thermal f_0 and non-thermal δf components, namely $f = f_0 + \delta f$. Thermal component f^0 is assumed to be Maxwellian with measured density and temperature and to be updated in each time step.

In this paper, a series of experiments have been performed to clarify experimentally the b-b Coulomb collision effect in LHD. We focus especially on the contribution of the b-b Coulomb collision effect to the fast velocity distribution by using TASK/FP. Since TASK/FP implements several Coulomb collision models, such as the nonlinear Coulomb collision model and the background Maxwell collision model, TASK/FP can separate the contribution of the b-b Coulomb collision effect from the simulation results. The details of the experiments will be explained in section 4.

The rest of this paper consists of the following. Analysis tools and models used in this paper are introduced in section 2. The description of the experimental apparatus is provided in section 3. The introduction of the experiment to evaluate the b-b Coulomb collision effect is explained in section 4. The result of the experiments and the simulation analyses are also provided in section 4. Discussion regarding the validity of the focus on the neutron decay time is found in section 5. Conclusion appears in section 6.

2. Analysis tools

The physics process investigated in this work uses the combination of the two simulation codes, FIT3D[20, 21, 22], and TASK/FP.

FIT3D code is composed of three components. The first component is a Monte Carlo code which calculates the fast ion birth profile (HFREYA). The second component is a Monte Carlo code which calculates radial redistribution of fast ions owing to the prompt orbit loss effect (MCNB). The distortion of the fast ion birth profile due to the finite orbit width effect is considered in this calculation. The third component is

a code which calculates analytically two dimensional (1D in radial direction and 1D in velocity space) steady state solution of the fast ion velocity distribution (FIT). FIT3D takes the plasma temperature and density profiles, the beam energy $E_{\rm beam}$, the beam port through power $P_{\rm beam}^{\rm port}$, and the 3D magnetic equilibrium as input. It is noted that since the neutral beam ionization is calculated by HFREYA, the observation data of the beam shine-through loss is not used in the present analysis.

TASK/FP is a three dimensional (2D in momentum space and 1D in radial direction) F-P code. It is used for the calculation of the evolution of the fast ion velocity distribution instead of FIT. Although TASK/FP has been developed originally as a full f prediction code, it is extended to calculate only non-thermal component of momentum distribution to use for experimental analyses. In the present analysis, the momentum distribution function is divided into two components, $f_s = f_s^0 + f_s^1$, where f_s^0 and f_s^1 denote the momentum distribution function of bulk and non-thermal components, and subscript s denotes "species." The bulk component f_s^0 is assumed to be Maxwellian with experimentally measured density $n_s^0(\rho, t)$ and temperature $T_s(\rho, t)$,

$$f_s^0(p) = \frac{n_s^0}{4\pi m_s^2 c T_s K_2(m_s c^2/T_s)} \exp\left(-\frac{m_s c^2 \gamma_s}{T_s}\right), \tag{1}$$

where $\gamma_s = (1 + p^2/m_s^2 c^2)^{1/2}$, c is the velocity of light, and K_n is the n-th order modified Bessel function of the second kind. The evolution of f_s^0 is not solved by the F-P equation but is replaced by eq. (1) in each time step. Only the non-thermal component f_s^1 is solved by the F-P equation as below:

$$\frac{\partial f_s^1}{\partial t} = \sum_{s'} C^{s/s'}(f_s^1, f_{s'}) + H, \tag{2}$$

$$C^{s/s'}(f_s^1, f_{s'}) = \nabla_p \cdot \left[\overleftrightarrow{\boldsymbol{D}}_C^{s/s'} \cdot \nabla_p f_s^1 - \boldsymbol{F}_C^{s/s'} f_s^1\right] \tag{3}$$

$$H = S_{\rm NB} - L_{\rm cx} - L_{\rm sink} \tag{4}$$

where ∇_p is a derivative operator in two dimensional momentum space (momentum p and pitch angle θ) and $C^{s/s'}$ is the Coulomb collision term, where superscript s and s' mean the incident and the background species, respectively. The tensor $\overleftrightarrow{\boldsymbol{D}}_C^{s/s'}$ and the vector $\boldsymbol{F}_C^{s/s'}$ denote the relativistic non-linear collisional diffusion and friction coefficients, whose expressions are given by Ref. [23]. The collision term is expanded by Legendre polynomial up to second order. In the present paper, H term includes the NB source term $S_{\rm NB}$, the charge exchange loss term $L_{\rm cx}$, and the particle sink term $L_{\rm sink}$, respectively. In the present analysis, TASK/FP takes the fast ion birth profile calculated by FIT3D as input. NB source term becomes $S_{\rm NB} = \partial f^{1,\rm abs}(p, \theta, \rho, t)/\partial t$. The charge exchange loss term, $L_{\rm cx}$, is given by:

$$L_{\rm cx}(\boldsymbol{p}_s) = n_n \sigma_{\rm cx}(E_s) v_s f_s^1(\boldsymbol{p}_s), \tag{5}$$

where n_n is the deuterium neutral gas density, E_s is the fast ion kinetic energy, and $v_s = p_s/m_s\gamma_s$. The charge exchange cross section $\sigma_{\rm cx}$ is also given by[24]:

$$\sigma_{\rm cx}(E_a) = \frac{0.6937 \times 10^{-18}(1 - 0155\log_{10}(E_a)^2)}{1 + 0.1112 \times 10^{-14} E^{3.3}} (\rm m^2). \tag{6}$$

The density of neutral gas, n_n, is assumed to be constant in time. Since the present version of TASK/FP can not take the data of the neutral gas density profile as input, the radial profile of the neutral gas is chosen to be:

$$\log_{10} n_n(\rho) = (\log_{10} n_n(0) - \log_{10} n_n(1)) \times (1 - \rho^{2.5})^{0.8} + \log_{10} n_n(1), \tag{7}$$

where $n_n(0) = 10^{14}$ m^{-3} and $n_n(1) = 10^{16}$ m^{-3}, respectively. This profile is assumed to be similar to the typical profile on LHD obtained by AURORA code[25]. The particle sink term, $L_{\rm sink}(f_s^1)$, is an artificial loss term. This term is intended to conserve the bulk density in order to maintain the density to the measured density by reducing fast ions which slow down to a few times of the thermal velocity, $v_{s,th} = \sqrt{T_s/m_s}$. This term is given by:

$$L_{\rm sink}(\boldsymbol{p}_s) = f_s^1/\tau_{\rm sink} \quad (\text{for } v_s < 3v_{s,th}), \tag{8}$$

where $\tau_{\rm sink} = 1.0$ ms is chosen. This value is sufficiently shorter than that of NB fast ion slowing down time. In the present TASK/FP analysis, radial transport during fast ion slowing down process is neglected. This means that fast ions are perfectly confined until they are thermalized.

The fusion reaction rate is calculated by:

$$S_n = \iint \sigma_{\rm nf}(E_{ab})\bar{v} f_a(\boldsymbol{p}_a) f_b(\boldsymbol{p}_b) d\boldsymbol{p}_a d\boldsymbol{p}_b, \tag{9}$$

where $E_{ab} \equiv 0.5 m_a m_b/(m_a + m_b)\bar{v}^2$ is the relative kinetic energy, $\bar{v} \equiv |\boldsymbol{v}_a - \boldsymbol{v}_b|$ is the relative velocity, and subscripts a, b indicate particle species, respectively. The fusion cross section $\sigma_{\rm nf}(E_{ab})$ is given by Ref. [26]. It is noted that the contribution of the fusion born tritons and helium ions to the deuteron velocity distribution is omitted in the present calculation because the fusion reaction rate is sufficiently low and omitting this contribution can accelerate the calculation. The reduction of fused deuterons is also not considered in the present simulation for the same reason.

3. Experimental apparatus

Figure 2 shows the schematic view of the NBI system on LHD. LHD is equipped with three tangential negative NBs (#1 - #3) and two radial positive NBs (#4-#5). NB#1 and #2 are hydrogen beams and NB#3 is a deuterium beam. In the following experiments, perpendicular NBs, NB#4 and NB#5, are not used. The typical values of beam energy, port through power, and beam ion species in the following experiment are illustrated in fig. 2. The toroidal magnetic field strength is $|B| = 2.75$ T, whose direction is counter-clockwise from the top view (the same direction as NB#1 and NB#3) and the preset of the magnetic axis position is $R_{\rm ax} = 3.6$ m. The plasma species is deuterium.

In the following experiments, we estimate the behavior of fast ions through the measurement of the neutron emission rate from the D-D reaction. Although the thermal-thermal fusion reaction will be dominant in the future reactor, like ITER, the beam-thermal reaction is dominant in LHD plasmas. Therefore, the neutron emission rate is

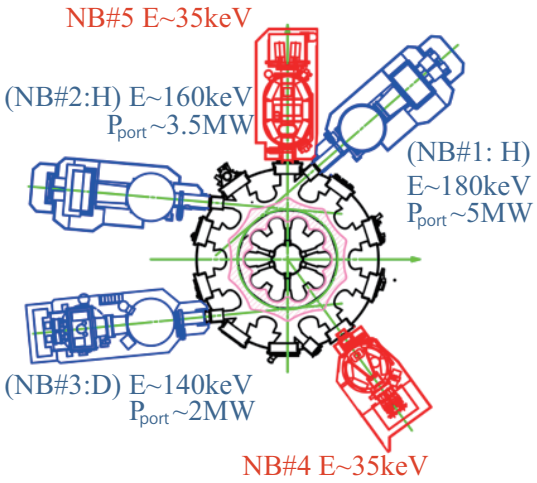

Figure 2. Top view of NBI systems on LHD. NB#1 to NB#3 are tangential negative-NBI and NB#4 and NB#5 are perpendicular positive-NBI. Perpendicular NBIs are not used in the present paper.

sensitive to the fast ion velocity distribution. In addition, since the cross-section of D-D fusion reaction increases monotonically with the increase of the beam energy within the range of the beam energy in LHD, the neutron emission rate reflects the slowing down of the fast ions. For these reasons, we can infer the fast deuteron velocity distribution from the observation of the neutron emission rate.

To observe the neutron emission rate, the Neutron Flux Monitor (NFM) has been installed[27] on LHD. It can measure the global neutron emission rate with fine temporal resolution.

4. Decay time of the neutron emission rate

In this paper, to investigate the contribution of the b-b Coulomb collision to the fast ion velocity distribution, we do not focus on the absolute value of the neutron emission rate, but on the neutron decay time after the deuterium beam has been turned off. This is because for the estimation of the neutron emission rate there are some uncertainties in the present experiment, such as the effective charge, the hydrogen to deuterium ratio, and the hydrogen to helium ratio. The absolute value of the neutron emission rate is sensitive to these uncertainties because the neutron emission rate is proportional to the bulk and fast deuteron densities. On the other hand, the neutron decay time is not sensitive to the uncertainties. This reason can be explained as below. The neutron decay time reflects the slowing down of NB fast deuterons. The slowing down of NB fast deuterons is not sensitive to the uncertainties because the slowing down of fast ions depends mainly on the electron density and the temperature, which can be measured. Therefore, the neutron decay time is more reliable than the absolute value of the neutron emission rate. The approach which focuses on the neutron decay time

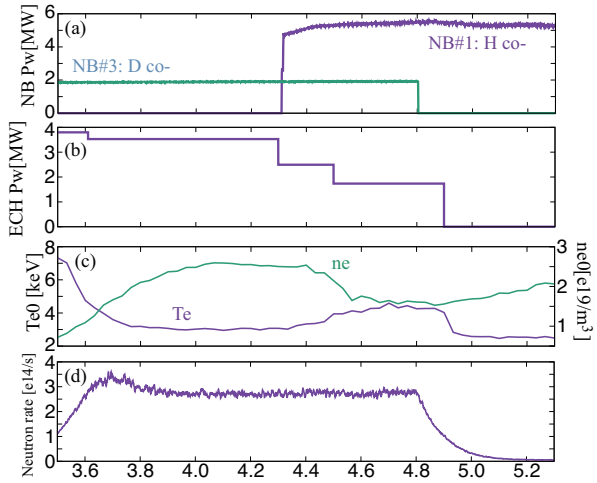

Figure 3. Typical waveform of "*co H*" case in this series of experiments (shot number: SN137352). The hydrogen beam is turned on at $t = 4.3$ sec and the deuterium beam is turned off at $t = 4.8$ sec.

has been adopted by previous works[28, 29] to investigate the NB fast ion slowing down process theoretically and experimentally. The details of the validity focusing on the neutron decay time will be discussed in sec. 5.

In the following sections, we investigate the contribution of the b-b Coulomb collision to the fast ion velocity distribution. To clarify the effect, we performed the following deuterium experiments on LHD. There are three tangential NBIs. One NBI is the deuterium beam and the other NBIs are hydrogen beams, which are in the opposite direction from each other, as shown in fig. 2. These three beams have similar kinetic energy $E_{\rm beam} \sim 140 - 180$ keV. In the experiments, the combination of the deuterium beam and one of the hydrogen beams was used. We use the hydrogen beam because the hydrogen beam does not contribute explicitly to the neutron emission rate. If the direction of the hydrogen beam has an influence on the neutron emission rate, this means that the velocity distribution of the NB fast deuteron is distorted due to the b-b Coulomb collision between proton and deuteron. For example, if the hydrogen beam has the same direction of the deuterium beam, it can be considered that the neutron decay time will be longer. This is because the velocity distribution of the NB fast deuteron is broadened to the high velocity direction due to the b-b Coulomb collision. On the contrary, if the hydrogen beam has the opposite direction of the deuterium beam, it can be considered that the neutron decay time is hardly affected by the NB fast protons. This is because the relative velocity between these two fast ions is too large to permit interaction with each other.

4.1. Experimental results

Figure 3 shows the typical waveform of this series of experiments. This figure indicates (a): NB port through power, (b): electron cyclotron heating (ECH) power, (c): electron

temperature and density on axis, and (d): neutron emission rate, respectively. ECH is used to control the electron temperature. Here, the typical error of the plasma parameter measurement is approximately less than 10%. We focus on the neutron decay time, $\tau_n^{\rm exp}$, after $t = 4.8$ sec when the deuterium beam is turned off. In the case shown, the hydrogen beam (NB#1), which has the same direction of the deuterium beam (NB#3), overlaps with NB#3. From here, we call this kind of case "co H injection," or simply "*co H.*" In addition, the case using NB#2 instead of NB#1 is called "counter H injection" or "*ctr. H.*" Finally, the case using no hydrogen beam is called "no H injection" or "*no H.*"

Here, we define the classical neutron decay time τ_n[28, 29], which is the e-folding time of the decay of the fusion reactivity due to the fast ion slowing down. The classical neutron decay time τ_n is derived theoretically by considering the fast ion deceleration from their injection energy, E_0, to the energy E_1, at which the fusion reactivity has fallen by $1/e$.

$$\tau_n \equiv \frac{\tau_{se}}{3} \ln \left(\frac{E_0^{3/2} + E_C^{3/2}}{E_1^{3/2} + E_C^{3/2}} \right), \tag{10}$$

$$\tau_{se} \equiv \frac{3(2\pi)^{3/2} \epsilon_0^2 m_D T_e^{3/2}}{n_e e^4 m_e^{1/2} \ln \Lambda}, \tag{11}$$

where $E_C \sim 18.6 T_e$ is the critical energy where ion drag is equal to electron drag, m_e and m_D are rest mass of electron and deuteron, and τ_{se} is the Spitzer beam slowing down time on electron. E_1 satisfies the following relation:

$$\frac{\sigma_{\rm nf}(E_1) v_1}{\sigma_{\rm nf}(E_0) v_0} \equiv \frac{1}{e}, \tag{12}$$

where v_0 and v_1 are satisfying $E_0 = m_D v_0^2/2$ and $E_1 = m_D v_1^2/2$. To estimate τ_{se}, we choose time averaged n_e and T_e during 100 ms after the deuteron beam is turned off on $\rho = 0.3$. The radial point $\rho = 0.3$ is chosen because the neutron emission around the point is dominant. The duration 100 ms is chosen because ECH injection continues at least 100 ms after the deuterium beam is turned off in all shots. In this duration, the plasma parameters do not change drastically, as shown in figure 3. For example, in fig. 3, the deuterium NBI is turned off at $t = 4.8$ s and the electron temperature and density maintain their value until $t = 4.9$s (T_e sharply drops after $t = 4.9$ s). In the present cases, the typical value of NB#3 injection energy is $E_0 \sim 140$ keV (Only NB#3 contributes explicitly to the fusion reaction) and $E_1 \sim 81.2$ keV, respectively. It is noted that the fast ion confinement is not considered at the derivation of τ_n though the classical fast ion deceleration is taken into account. Since the fast ion confinement time is not infinity in real plasmas, τ_n tends to be longer than the experimentally observed neutron decay time.

Figure 4 shows the decay time of the neutron emission rate, $\tau_n^{\rm exp}$, against to the classical neutron decay time, τ_n in each shot. Circle, square, and rhombus points indicate "co H," "ctr. H," and "no H" cases, respectively. In fig. 4, the value of $\tau_n^{\rm exp}$ is estimated by a curve fitting to $g(t) = C \times \exp(-t/\tau_n^{\rm exp})$ during 100 ms after the deuteron beam is turned off.

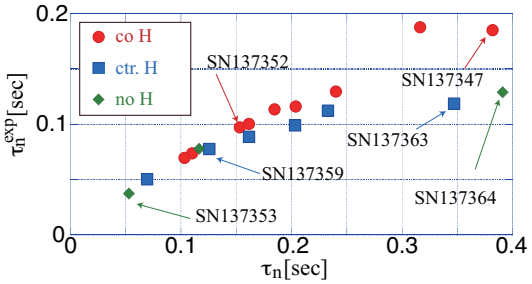

Figure 4. The decay time of the neutron emission rate in experiment, $\tau_n^{\exp}$, against to the classical neutron decay time, τ_n, is displayed. Circle, square, and rhombus points indicate "co H," "ctr. H," and "no H" cases, respectively. This figure includes 18 shots on LHD.

From fig. 4, it is found that $\tau_n^{\exp}$ separates from τ_n as τ_n increases among three cases. This tendency can be roughly grasped by the following expression:

$$(\tau_n^{\exp})^{-1} \sim \tau_n^{-1} + \tau_c^{-1}, \tag{13}$$

where τ_c denotes the fast ion confinement time, which has been omitted at the derivation of τ_n. In D-D reaction cases, the fast ion slowing down and the fast ion loss cause the decay of the fusion reactivity. Here, the term "fast ion loss" indicates the actual spatial transport. The first and second terms of eq. (13) describe the neutron decay due to the fast ion slowing down and the fast ion loss, respectively. When the fast ion slowing down is sufficiently faster than the fast ion loss, the experimental neutron decay time is decided mainly by τ_n. In the contrary case, when the fast ion slowing down is sufficiently slower than the fast ion loss, the experimental neutron decay time is decided by the fast ion confinement time. Therefore, it can be considered that the experimental neutron decay time obeys $\tau^{\exp} \sim \tau_n$ in the low τ_n region and approaches gradually to the fast ion confinement time, $\tau_n^{\exp} \sim \tau_c$, as τ_n increases.

From fig. 4, it is also found that the experimental neutron decay time of the "co H" case becomes longer than that of the "*ctr. H*" case and the "*no H*" cases, as predicted above. It can be considered that there are two possible factors which cause the difference between "*co H*" and the other two cases. One reason is that the fast ion loss may be different among the three cases with the same τ_n. This is because the beam port through power is different between NB#1 and NB#2 for EP driven instabilities. The difference of the beam port through power causes the difference of the fast ion pressure gradient. In addition, the presence of co-direction H beam affects the fast deuteron pitch angle distribution. The distortion of the pitch angle distribution influences the neo-classical transport. As a result, the fast ion loss among the three cases are different from each other. The other factor is the contribution of the b-b Coulomb collision as noted above. Since the b-b Coulomb collision effect is not influenced explicitly by the bulk density and temperature but by the fast ion density, this effect is independent explicitly from τ_n. Therefore, the contribution of the b-b Coulomb collision is clarified in the long τ_n region.

In the following section, since it is too difficult to estimate EP transport without instability analysis, we aim to estimate the contribution of the b-b Coulomb collision using Fokker-Planck simulation.

4.2. Simulation results

To simulate the evolution of the neutron emission rate using TASK/FP, the following assumptions are adopted. Since the ion temperature is not measured in the present experiments, it is assumed to be the same as the electron temperature, namely $T_e = T_i$. The ratio of bulk proton and deuteron densities are assumed to satisfy $n_D^0/(n_D^0 + n_H^0) = 0.9$. The superscript 0 indicates the bulk components. The effective charge is assumed to be $Z_{\rm eff} = 2$ in the whole plasma and the whole discharge. Here, carbon ion is assumed to be impurity. Ion densities are composed of the bulk and the fast ion densities, that is $n_D = n_D^0 + n_D^1$ and $n_H = n_H^0 + n_H^1$. However, the fast ion densities n_D^1 and n_H^1 are not taken into account in the charge neutrality; $n_e = n_D^0 + n_H^0 + 6n_C$. Because of this reason, the total deuteron and proton densities and the neutron emission rate are over-estimated. The fast ion densities are given by $n_s^1 = \int f_s^1 d\boldsymbol{p}$. The contribution of fusion born protons and tritons to the deuteron velocity distribution are neglected because the DD reaction rate is sufficiently low. Since we focus on the tangential deuterium beam, the trapped particle effect is omitted. In the following calculation, the time evolutions of fast proton velocity distribution f_H^1 and the fast deuteron velocity distribution f_D^1 are calculated. The time evolutions of the electron and carbon velocity distribution are not calculated and are assumed to be Maxwellian, that is $f_e = f_e^0$ and $f_C = f_C^0$. Impacts of these assumptions to the simulation results are discussed in sec. 5.

Figure 5 shows the evolutions of the observed and simulated neutron emission rate in six shots indicated in figure 4. Although the deuterium NBI begins at $t = 3.3$ sec, these calculations start at $t = 3.31$ sec because of the lack of data at $t = 3.3$ sec. Red solid curve indicates the experimental result of the neutron emission rate. Green dashed and blue dotted curves denote the simulation results including the deuteron-proton b-b Coulomb collision effect and those excluding the deuteron-proton b-b Coulomb collision effect, respectively. The difference between these two simulations comes from the difference of the Coulomb collision term $C^{s/s'}(f_s, f_{s'})$. In the case including the deuteron-proton b-b Coulomb collision effect, the Coulomb collision term becomes $\sum_{s'} C^{s/s'}(f_s^1, f_{s'})$ where s' includes electron, proton, deuteron, and carbon ion. On the other hand, in the case excluding the deuteron-proton b-b Coulomb collision, the background proton velocity distribution is Maxwellian only when the incident species is deuteron, namely: $\sum_{s''} C^{D/s''}(f_D^1, f_{s''}) + C^{D/H}(f_D^1, f_H^0)$, where s'' includes electron, deuteron, and carbon ion. If the incident species is proton, the collision term is $\sum_{s'} C^{H/s'}(f_H^1, f_{s'})$. Both of these two collision models include the deuteron-deuteron b-b Coulomb collision. Excluding the deuteron-proton b-b Coulomb collision model is intended to reduce the contribution of the fast protons to the deuteron velocity distribution in order to clarify the deuteron-proton b-b Coulomb collision effect. For

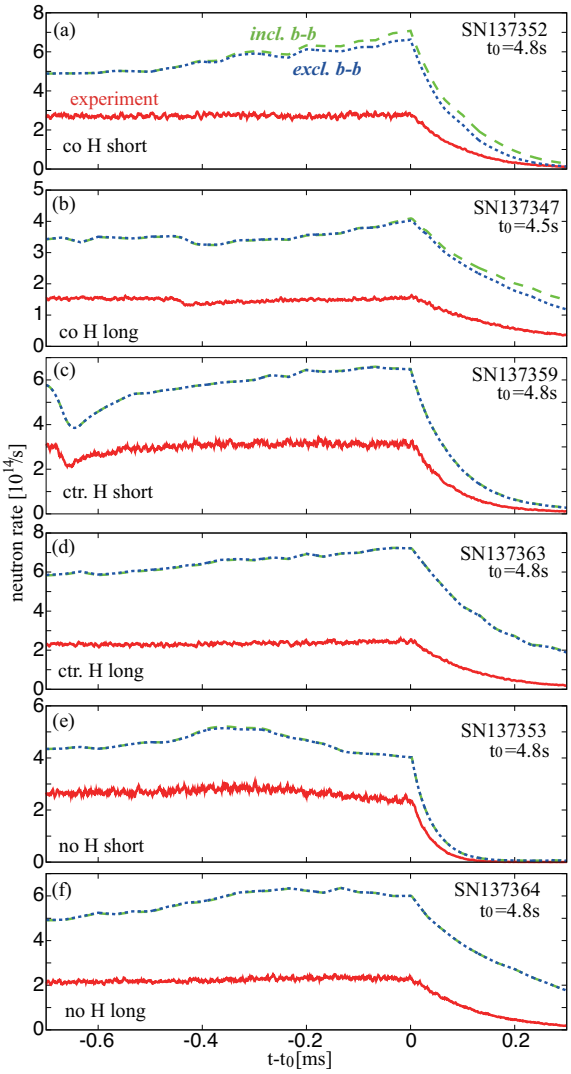

Figure 5. Evolutions of the neutron emission rate in six shots (indicated in fig. 4) are shown. Red solid, green dashed, and blue dotted curves denote the results of experiment and simulations including or excluding the deuteron-proton b-b Coulomb collision effect, respectively. Deuterium beam is turned off at $t = t_0$. The value of t_0 in each shot is displayed in each figure.

simplicity, we call these two simulations cases as *incl. b-b* and *excl. b-b*.

Since the present F-P calculations do not include the fast ion loss mechanism such as classical, neo-classical and EP driven instabilities, the simulated values of the neutron emission rate are higher than those of the measured neutron emission rate in each case, as expected. It is noted, however, that the fast ion loss during fast ion birth process, such as prompt loss and beam shine through, is included as noted in sec. 2. From fig. 5 (c)-(f), it is found that there is no difference between *incl. b-b* and *excl. b-b* cases. This means the deuteron-proton b-b Coulomb collision has no contribution to the deuteron velocity distribution except *co H* cases.

The measured and two simulated neutron decay times are listed in table 1, where

SN	label	τ_n	$\tau_n^{\rm exp}$	$\tau_n^{incl.}$	$\tau_n^{excl.}$
137352	co H	0.15	0.097	0.10	0.089
137347	co H	0.38	0.19	0.24	0.22
137359	ctr. H	0.13	0.078	0.084	0.084
137363	ctr. H	0.35	0.12	0.19	0.18
137353	no H	0.053	0.037	0.040	0.040
137364	no H	0.39	0.13	0.22	0.22

Table 1. The classical neutron decay time τ_n, the decay time of the measured and two kinds of simulated neutron emission rates $\tau_n^{\rm exp}$, $\tau_n^{incl.}$, and $\tau_n^{excl.}$ are tabulated in six shots. The dimension of these values are second.

$\tau_n^{incl.}$ and $\tau_n^{excl.}$ denote the simulated neutron decay time of *incl. b-b* and *excl. b-b* cases. In short τ_n cases (SN137352, SN137359, and SN137346), $\tau_n^{\rm exp}$ and $\tau_n^{incl.}$ have a good agreement because the contribution of collisional slowing down is sufficiently stronger than that of fast ion loss. Note that since the "*excl. b-b*" case does not include the deuteron-proton b-b Coulomb collision effect, which is included in actual plasmas, the value of $\tau_n^{excl.}$ can be less than $\tau_n^{\rm exp}$. In long τ_n cases, on the contrary, the differences between $\tau_n^{\rm exp}$ and $\tau_n^{incl.}$ are not negligible. In "*ctr. H*" and "*no H*" cases, there are minute differences between $\tau_n^{incl.}$ and $\tau_n^{excl.}$. This result means that the deuteron-proton b-b Coulomb collision does not affect the fast deuteron velocity distribution in "*ctr. H*" and "*no H*" cases as predicted above. On the other hand, in "*co H*" cases, it is found that there are meaningful differences between two simulated values. This means that the presence of the deuteron-proton b-b Coulomb collision extends the simulated neutron decay time $\tau_n^{incl.}$. Figure 6 shows the energy distributions of f^1 one dimensionally against to the energy in the deuteron beam direction ($\theta \sim 0.17$ radian) at $t - t_0 = 0$ ms and 200ms in the three long τ_n cases. This figure clarifies the contribution of the deuteron-proton b-b Coulomb collision to the energy distribution. In figure 6-(a), green curves, which denote f^1 of *incl. b-b* case, are accelerated rather than blue curves owing to the deuteron-proton b-b Coulomb collision. Conversely, in figures 6-(b) and (c), there is little difference between green and blue curves.

The simulation results are plotted on figure 7 with the experiment data, which have already been shown in fig. 4. The simulation result shows the similar tendency that the decay time of the neutron emission rate of "*co H*" case is longer than the other two cases in long τ_n region. From simulation results shown in figs. 5, 6, and 7 it is found that the b-b Coulomb collision effect has a meaningful contribution to the decay time of the neutron emission rate. However, since the difference of $\tau_n^{\rm exp}$ around $\tau_n \sim 0.35$ between "*co H*" and the other two cases is larger than the difference of $\tau_n^{incl.}$ between "*co H*" and the other two cases, the contribution of the b-b Coulomb collision to the decay time is insufficient to explain the experimental results, as shown in fig. 7. It is considered that the fast ion loss, which is omitted in the present simulation, may be different between the "*co H*" case and the other two cases.

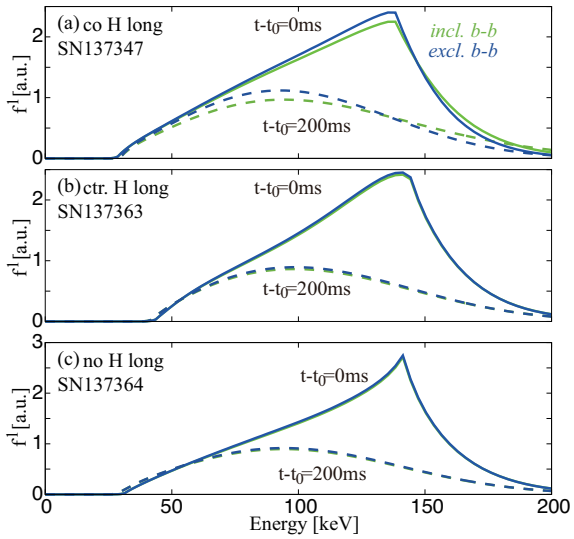

Figure 6. Energy distribution of the deuteron fast ion in the deuteron beam direction ($\theta \sim 0.17$ radian) are shown. Green and blue curves denote f^1 of *incl. b-b* and *excl. b-b* cases. The particle sink term, expressed in eq. (8), exists within $E <\sim 15 - 20$ keV.

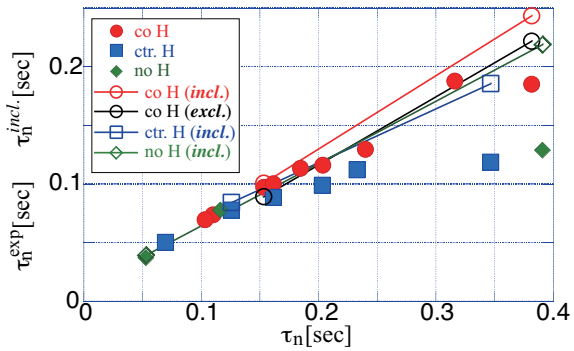

Figure 7. The decay time of the neutron emission rates $\tau_n^{\rm exp}$ and $\tau_n^{\rm sim}$ against to the classical neutron decay time τ_n is shown. Open circles and boxes with lines denote the simulation results.

5. Validity of focusing on the decay time

As discussed in the first paragraph in sec. 4, the deuteron ratio and the effective charge strongly affect the fusion reactivity, which is proportional to the deuteron bulk density. The neutron decay time, however, is not sensitive to the uncertainty of the deuteron density because the decay of the fusion reactivity due to the fast ion slowing down mainly depends on the electron density and the temperature, especially in the region where the energy of the fast ion is greater than the critical energy E_C. In most of the present experiments, the time averaged electron temperature on $\rho = 0.3$ during 100 ms after the deuterium beam is turned off is less than 4 keV (Only two cases reach to 4.2 and 4.4 keV). Then, the energy E_1 satisfies $E_C \lesssim E_1$ in most of the present analyses.

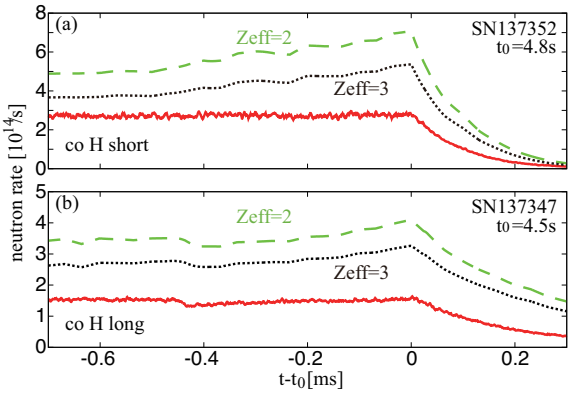

Figure 8. Evolutions of the neutron emission rate in two shots ("*co H*" case). Green dashed and black dotted curves denote $\tau_n^{incl.}$ with $Z_{\rm eff} = 2$ and 3.

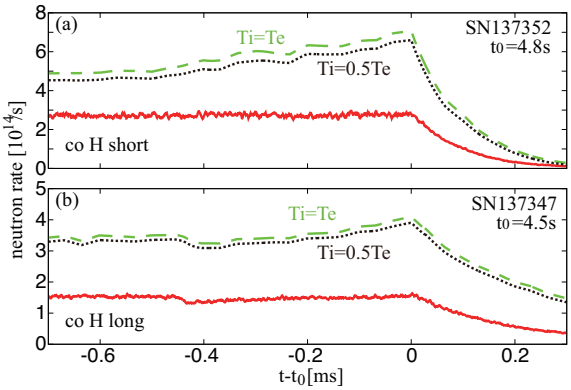

Figure 9. Evolutions of the neutron emission rate in two shots ("*co H*" case). Green dashed and black dotted curves denote $\tau_n^{incl.}$ with $T_i = T_e$ and $T_i = T_e/2$.

Figure 8 shows the evolutions of the neutron emission rate in two shots ("*co H*" case). Green dashed and black dotted curves denote $\tau_n^{incl.}$ with $Z_{\rm eff} = 2$ and 3. It is found that the absolute value of the neutron emission rate with $Z_{\rm eff} = 3$ is reduced by $\sim 20\%$ than that with $Z_{\rm eff} = 2$. On the other hand, their decay time are not sensitive to $Z_{\rm eff}$. For example, the simulated neutron decay time in short τ_n case (SN137352) are $\tau_n^{incl.} = 0.10$, $(ZEFF = 2)$ and $\tau_n^{incl.} = 0.10$, $(ZEFF = 3)$. And the simulated neutron decay times in long τ_n case (SN137347) are $\tau_n^{incl.} = 0.24$, $(ZEFF = 2)$ and $\tau_n^{incl.} = 0.25$, $(ZEFF = 3)$, respectively. According to these results, we consider that the contribution of the bulk ion uncertainties to the neutron decay time is sufficiently small in the present analysis.

In addition, though the ion temperature is assumed to be same as the electron temperature, it can be considered that the electron temperaure is higher than the ion temperature beucase the present plasmas are heated by ECH, as shown in fig. 3. It is known that the beam-thermal fusion reactivity increases with the ion bulk temperature[30]. Therefore, the assumption of $T_e = T_i$ also leads to over-estimation of

the neutron emission rate. Figure 9 shows the evolutions of the neutron emission rate in two shots ("*co H*" case). Green dashed and black dotted curves denote $\tau_n^{incl.}$ with $T_i = T_e$ and $T_i = T_e/2$ assumptions. It is found that the absolute value of the neutron emission rate with $T_i = T_e/2$ is reduced by $\sim 5\%$ than that with $T_i = T_e$. The neutron decay time is reduced by a few percentages. For example, the simulated neutron decay times in short τ_n case (SN137352) are $\tau_n^{incl.} = 0.10$, $(T_i = T_e)$ and $\tau_n^{incl.} = 0.095$, $(T_i = T_e/2)$, and that in long τ_n case (SN137347) are $\tau_n^{incl.} = 0.24$, $(T_i = T_e)$ and $\tau_n^{incl.} = 0.24$, $(T_i = T_e/2)$, respectively. From this result, it can be considered that the neutron decay time is not sensitive to the uncertainty of the ion temperature.

According to these results, focusing on the neutron decay time is valid rather than focusing on the neutron emission rate itself.

6. Conclusion

In this paper, a series of experiments and simulation analyses have been performed to investigate the contribution of the beam-beam (b-b) Coulomb collision effect to the fast ion slowing down process. In these experiments, the deuterium plasma is heated by both hydrogen and deuterium tangential NBIs. To evaluate the b-b Coulomb collision effect, we focused on the decay time of the neutron emission rate in deuterium plasma after the deuterium NBI has been turned off. If the hydrogen beam has the same direction of the deuterium beam ("*co H*" case), it is expected theoretically that the decay time of the neutron emission rate becomes longer than that with the opposite direction hydrogen beam ("*ctr. H*" case). This is because the deuteron velocity distribution is broadened to high velocity region due to b-b Coulomb collision. On the other hand, if the hydrogen beam has an opposite direction of the deuterium beam, it is also expected theoretically that the fast protons do not interact with the fast deuterons due to their high relative velocity. To confirm this prediction, a series of experiments have been performed.

From the experimental results shown in fig. 4, it is found that the difference of the hydrogen beam direction influences the decay time of the neutron emission rate $\tau_n^{\exp}$. There are two possible factors causing these different tendencies of the decay time of the neutron emission rate. One is the b-b Coulomb collision effect, the other is the fast ion loss effect. Since the fast ion loss mechanism is too complicated to estimate without instability code, in the present paper we aimed to estimate the contribution of the b-b Coulomb collision effect by using Fokker-Planck (F-P) code.

The simulation results are plotted on fig. 7 with the experiment data, which are already shown in fig. 4. It is noted that since our F-P simulation ignores the fast ion loss during fast ion slowing down process, the neutron emission rate and its decay times are over-estimated. From simulation results shown in figs. 5 and 6 it is found that the b-b Coulomb collision effect has a meaningful contribution to the decay time of the neutron emission rate. However, since the difference of $\tau_n^{\exp}$ around $\tau_n \sim 0.35$ between "*co H*" and the other two cases is larger than the difference of simulated values between "*co H*" and the other two cases, the contribution of the b-b Coulomb collision does not seem to

be fundamental for the interpretation of the experimental results. It is considered that the fast ion loss, which is omitted in the present simulation, may be different between the "*co H*" case and the other two cases. To proceed with the analysis, experiments in which fast ion loss is suppressed as much as possible or analyses including fast ion loss due to the neo-classical mechanism and fast ion driven instabilities are required. These are future works.

Acknowledgments

This work is supported partly by LHD project budgets (NIFS17KLPT005). It has been performed on "Plasma Simulator" (FUJITSU FX100) of NIFS with the support and under the auspices of the NIFS Collaboration Research program (NIFS16KNSR005).

[1] W. Heidbrink, N. Gorelenkov, Y. Luo, et al.: Physical review letters **99** (2007) 245002.
[2] R. White, N. Gorelenkov, W. Heidbrink, et al.: Physics of Plasmas **17** (2010) 056107.
[3] Y. Todo, M. Van Zeeland, A. Bierwage, et al.: Nuclear Fusion **54** (2014) 104012.
[4] Y. Todo, M. Van Zeeland, W. Heidbrink: Nuclear Fusion **56** (2016) 112008.
[5] W. Heidbrink, C. Collins, M. Podestà, et al.: Physics of Plasmas **24** (2017) 056109.
[6] H. Nuga, A. Fukuyama: Progress in Nuclear Science and Technology **2** (2011) 78.
[7] H. Nuga, M. Yagi, A. Fukuyama: Physics of Plasmas **23** (2016) 062506.
[8] S. Murakami, U. Gasparino, H. Idei, et al.: Nuclear Fusion **40** (2000) 693.
[9] S. Murakami, H. Yamada, M. Sasao, et al.: Fusion science and technology **46** (2004) 241.
[10] M. Osakabe, S. Murakami, M. Yoshinuma, et al.: Review of Scientific Instruments **79** (2008) 10E519.
[11] H. Yamaguchi, S. Murakami: Plasma and Fusion Research **9** (2014) 3403127.
[12] C. Karney: Computer Physics Reports **4** (1986) 183.
[13] R. Harvey, M. McCoy. "The CQL3D Fokker-Planck Code". `http://www.compxco.com/cql3d.html`, 2005.
[14] J. McKenzie, M. O'Brien, M. Cox: Computer Physics Communications **66** (1991) 194.
[15] M. Brambilla: Nuclear fusion **34** (1994) 1121.
[16] M. Schneider, L.-G. Eriksson, T. Johnson, et al.: Nuclear Fusion **55** (2014) 013003.
[17] M. Weiland, R. Bilato, R. Dux, et al.: Nuclear Fusion **58** (2018) 082032.
[18] A. Fukuyama. "TASK code Home Page". `http://bpsi.nucleng.kyoto-u.ac.jp/task/`.
[19] M. Yokoyama, R. Seki, C. Suzuki, et al.: Nuclear Fusion **57** (2017) 126016.
[20] S. Murakami, N. Nakajima, M. Okamoto. Fusion Technology 27 Suppl, 1995.
[21] M. Sato, S. Murakami, A. Fukuyama, et al.: Proc. 18th Int. Toki Conf, 2008.
[22] P. Vincenzi, T. Bolzonella, S. Murakami, et al.: Plasma Physics and Controlled Fusion **58** (2016) 125008.
[23] B. Braams, C. Karney: Phys. Fluid B **1** (1989) 1355.
[24] R. L. Freeman, E. M. Jones. Culham Report CLM-R 137. UKAEA Research Group 1974.
[25] M. Hughes, D. Post: Journal of Computational Physics **28** (1978) 43.
[26] H.-S. Bosch, G. Hale: Nuclear Fusion **32** (1992) 611.
[27] M. Isobe, K. Ogawa, H. Miyake, et al.: Review of Scientific Instruments **85** (2014) 11E114.
[28] J. Strachan, P. Colestock, S. Davis, et al.: Nuclear Fusion **21** (1981) 67.
[29] W. Heidbrink, J. Kim, R. Groebner: Nuclear fusion **28** (1988) 1897.
[30] D. Mikkelsen: Nuclear Fusion **29** (1989) 1113.